Surface & Coatings Technology 205 (2011) 5437–5443

Contents lists available at ScienceDirect

Surface & Coatings Technology

journal homepage: www.elsevier.com/locate/surfcoat

Structural considerations in plasma spraying of the alumina–zirconia composite

F. Tarasi [a], M. Medraj [a,*], A. Dolatabadi [a], J. Oberste-Berghaus [b,1], C. Moreau [b]

[a] Mechanical Engineering Department, Concordia University, Montreal, Quebec, Canada
[b] National Research Council Canada, Industrial Materials Institute, Boucherville, Quebec, Canada

ARTICLE INFO

Article history:
Received 15 October 2010
Accepted in revised form 8 June 2011
Available online 16 June 2011

Keywords:
Atmospheric plasma spray
Amorphous phase
Ceramic nano-composite
Supersaturated solid solutions
Melting and mixing

ABSTRACT

The focus of this study is the amorphous and crystalline phase formation in air plasma sprayed alumina–yttria stabilized zirconia coatings. In this multi-component system at compositions close to its eutectic, amorphous structures can arise by virtue of the high cooling rates of melted particles. Two avenues for amorphous phase formation have been identified: in-flight and upon-impact mixing. While the crystalline structure is largely retained by unmelted or partly melted feed particles embedded in the coating, it can also be created in the solidification process. The formation of a supersaturated crystalline phase is proposed. It was found that the formation of the crystalline phases with supersaturated composition in alumina–YSZ composite is possible, in spite of the high cooling rates during spray process.

1. Introduction

Air plasma spraying (APS) is a well established coating process offering high production rate at relatively low costs. Different aspects of this technology have been summarized by, for example, Fauchais et al. [1–3]. An important application of APS is the production of thermal barrier coatings (TBCs) [4–6]. Yttria stabilized zirconia materials (YSZ) are commonly applied. As an alternative, alumina-stabilized zirconia composites have been studied [7–10]. An interesting feature of thermal sprayed alumina–zirconia is the formation of non-crystalline phases [11,12], which are invoked by the high cooling and solidification rates of the, so called, splats. Based on heat transfer calculations, Kim et al. [12] reported cooling rates of about 10^6 K/s. Significantly higher cooling rates of $(100 \text{ to } 600)\times10^6$ K/s are proposed by Fauchais et al. [2], based on experimental results. These cooling rates are in agreement with McDonald et al. [13] reporting approximately 10^7 K/s. Although, the cooling of the splats depend on a number of variables, such as material, particle size and substrate conditions, very high cooling rates can prevent the atoms to order into a crystalline structure during solidification. There are even reports of almost fully amorphous alumina–zirconia coatings produced by APS [12,14].

In order to control the amount of amorphous and crystalline phases in the coating, which can influence the coating properties, it is important to further understand their mechanism of formation. This work investigates various origins of the amorphous or crystalline structures using two very different types of powders, i.e. spray-dried and fused and crushed composites. As-sprayed coatings and in-flight collected particles are considered.

2. Experimental

Two different powders were used in the present work. The spray-dried Powder 1, with a composition of 60 wt.% alumina and 40 wt.% of 3YSZ (3 mol% yttria stabilized zirconia), is in the form of nano-particulates agglomerated into ~45 μm size particles. The powder is supplied by Tosoh Inc., Grove City, OH, USA as TZ3460A. Powder 2 (60/40 wt.% Al_2O_3/ZrO_2) are fused and crushed particles with a nominal size of 5 to 22 μm. It is supplied by H.C. Starck, Sarnia, ON, Canada as Amperite750. Fig. 1 shows the morphology of the feed powders. Powder 1 is approximately three times larger than Powder 2. The inset micrograph of Fig. 1(a), showing a magnification of the agglomerates, illustrates a large number of small pores between constituent particulates.

This figure also suggests that the particulates are only loosely connected within the agglomerate. Fig. 1(b) depicts the fused and crushed particles of Powder 2, with sharp corners, suggesting a denser structure. XRD analysis showed that Powder 2 is composed of monoclinic and tetragonal zirconia (with no trace of stabilizing agents, e.g. yttria), and α- and γ-alumina. Powder 1, on the other hand, contains only tetragonal YSZ and γ-alumina.

The powders were axially injected into Mettech Axial III (Northwest Mettech Corp. North Vancouver, BC, Canada) plasma torch and were sprayed under the conditions summarized in Table 1. The dry powder was injected at a feed rate of 21 g/min using an argon carrier gas flow of 6 slm. Coatings were deposited on mild steel coupons (2.5×2.5 cm^2 with 0.5 cm thickness), pre-coated with a NiCrCoAlY bond coat. The coatings were produced in 12 deposition passes. The in-flight particle

* Corresponding author.
E-mail address: mmedraj@encs.concordia.ca (M. Medraj).
[1] Current address: Bekaert Advanced Coatings NV, Belgium.

0257-8972/$ – see front matter © 2011 Elsevier B.V. All rights reserved.
doi:10.1016/j.surfcoat.2011.06.016

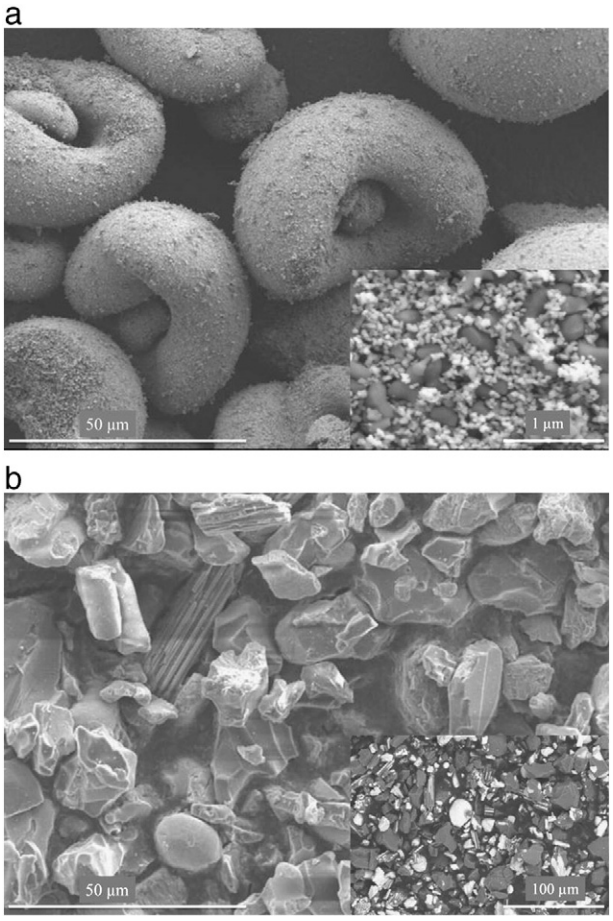

Fig. 1. Feed powders, a) Powder 1 at about 1kX and the inset micrograph is at 50kX; b) Powder 2 at 1kX and inset micrograph is at 500X in back scattered mode.

temperature (T_p) and velocity (V_p) were measured with a DPV2000 (Tecnar Automation Limited, St Bruno, QC, Canada). The field of view of the sensor head was positioned in the center of the particle jet at the same spray distance as used for deposition. Results of the measured particle states are summarized in Table 1.

In-flight particles were collected after each coating deposition by directing the spraying torch into a large water reservoir. The torch was held at a distance of 30–50 cm above the water surface for approximately 1 min. This distance was necessary to prevent splashing water to reach the torch. The collected particles were then air-dried. An SEM (Hitachi S4700 GCEMarket, Inc. Blackwood, NJ, USA) was used to analyze particle morphology and chemical composition using energy dispersive X-ray spectrometry (EDS). For a cross-sectional view, the particles were embedded in a resin and then polished together with the mount. The particle size distribution was determined with a laser diffraction particle size analyzer LS3 320 (Beckman Coulter, Miami, Fl, USA).

XRD measurements were conducted with a Bruker D8-Discovery diffractometer (Bruker AXS, Inc., Madison, WI, USA). The amorphous phase content in the samples was evaluated by the area ratio of the amorphous hump to the crystalline peaks in the range of 20° to 90°. This ratio is denoted here as the amorphous index, being the reciprocal of the crystallinity index (CI), which is the ratio of the Bragg's peaks to the total area of peaks and humps within a specific 2θ range [15]. In addition, differential scanning calorimetric (DSC) measurements were conducted to evaluate the amount of amorphous phase using a TG96 apparatus (Setaram Inc., Newark, Ca, USA) [11,12,16]. A heating rate of 5 °C/min was used. Comparison of the areas of the crystallization peaks allowed a relative measure of the amorphous content in the different samples,

To gain further insight into the crystalline structure of the coatings, Rietveld analysis using PowderCell [17] was applied to estimate the unit cell parameters, as will be discussed later.

Table 1
Spray condition for the two types of powders and the resulting particle conditions and coating thicknesses.

Spray condition / Sample	Total gas (slm)	Plasma current (amperes)	Gas composition ($Ar/N_2/H_2$)	Spray distance (mm)	$T_p \pm 20$ (°C)	$V_p \pm 10$ (m/s)	Coating thickness (mm)
Powder 1	120	200	10/80/10	100	2250	222	463
Powder 2					2455	245	303

3. Results and discussions

3.1. In-flight particle states

Fig. 2 shows in-flight particle temperatures for Powder 2 as a function of distances from the torch exit nozzle. A steep decrease in particle temperature can be seen. Extrapolating linearly to the water surface at a spray distance of 30–50 cm, the collected particles have possibly cooled below the melting point of their lowest-melting constituent before they enter the water ($T_{melting} = 2050$ °C for alumina). By consequence, they have solidified in-flight at low cooling rates. A similar trend is assumed for Powder 1, due to almost identical compositions. However, the particle size difference between the powders may result in a different number of in-flight solidified particles collected.

Analysis of the particle size distribution of the collected powders shows an average size of 46 μm (14–90 μm range) for Powder 1 and 15 μm (6.7–23 μm range) for Powder 2, almost the same as for the initial feeds. The negligible size change before and after spraying indicates that no significant fragmentation has occurred in the plasma. In particular, the loosely packed sprayed dried particles retained integrity.

The microstructures of the collected particles from the two types of powders are compared in Fig. 3. Due to initially well-mixed particulates of the two components (alumina and YSZ), Powder 1 yields sprayed particles of rather uniformly mixed composition. The collected particles from this powder shown in Fig. 3(a) contain large and small pores. These particles can be categorized as unmolten, partlymolten and fully molten particles, which are shown in Fig. 4. The unmolten particles, as in Fig. 4(a), are still porous but with larger

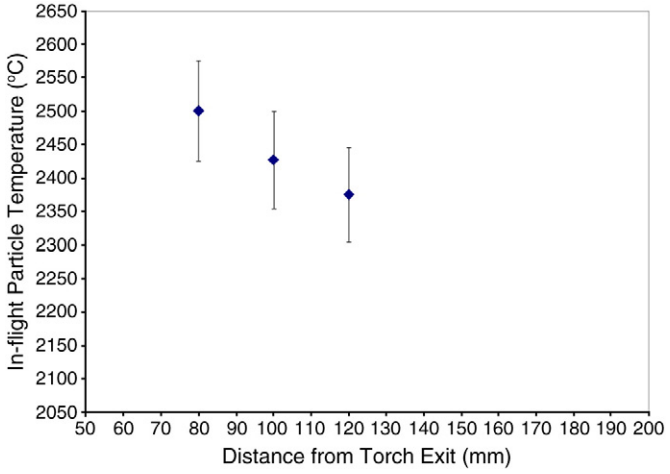

Fig. 2. Variation of particle temperatures with the distance from the torch exit nozzle for Powder 2.

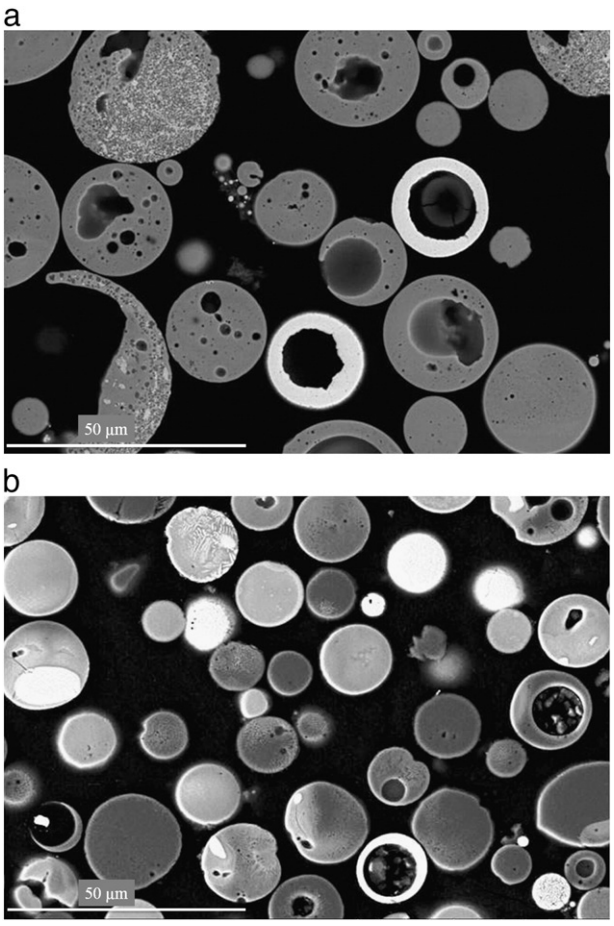

Fig. 3. Cross section of the mounted and polished in-flight particles collected into water after spraying under similar plasma spray condition a) Powder 1 and b) Powder 2.

particulates than the initial powder. This increase in particulate size could be attributed to in-flight sintering.

Fully molten and solidified particles, indicated in Fig. 4(b), are dense with mostly large pores in the center. Fig. 4(c) is an enlarged view of a partially molten particle. The figure illustrates how the transition from porous to hollow sphere could occur. As the melting starts from the surface, the progressing melt front sweeps up the submicron pores, which then eventually coalesce. This leaves several large pores in the melt, which may merge into a single pore in the center to forma shell-like particle. This shell formation may account for the negligible change in particle size observed between the initial and collected powder.

While the majority of the submicron size pores are annihilated into larger pores, many of them are still dispersed within the molten particle. Such porosity, transferred from the porosity of the feed, plays an interesting role in the phase composition of the solidified particle, which will be discussed later.

Fig. 5 shows the collected particles from the fused and crushed Powder 2. Based to their spherical shape, these particles have been almost completely molten during spraying, but with a variety of mixing behavior. They can be categorized as fully unmixed single component, partly mixed and fully mixed particles. The unmixed single component particle is either a white YSZ particle or dark alumina particle. Fig. 5(a) shows dendritic solidification, most common for those single component particles. In the partly mixed particles of Fig. 5(b), only the grains of unmixed portions are dendritic. In the mixed areas of a particle or in the fully mixed particles no grain can be seen. Ultra-high magnification of the fully mixed particle at

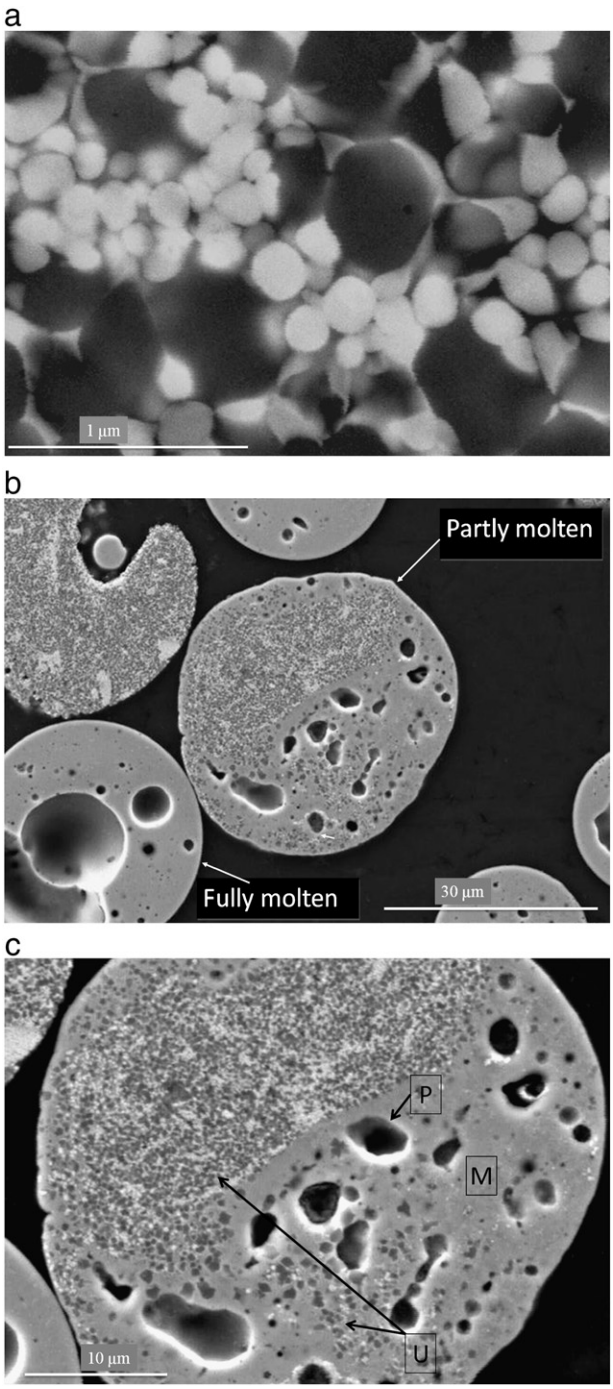

Fig. 4. Powder 1 collected particles a) unmolten particle; b) fully molten-resolidified andpartly molten c) partly molten particle consisting of unmolten region indicated by U, molten region, M and enlarged pores designated by P.

50kX by SEM in Fig. 5(c) presents no signs of crystalline grains, which suggests that these structures may be amorphous.

Particles with complete melting and mixing were the most common category observed in both types of powder. Fig. 6 is an SEM micrograph with EDS elemental mapping of the same particle observed in Fig. 5(c). It shows almost complete homogeneity in composition and a uniform distribution of aluminum and zirconium atoms. Since alumina and zirconia have very low mutual solid solubility, this could have only happened after complete melting. Although Figs. 5 and 6 belong to Powder 2, a similar lack of crystal grains and uniform elemental distribution was seen in the fully molten particles of Powder 1.

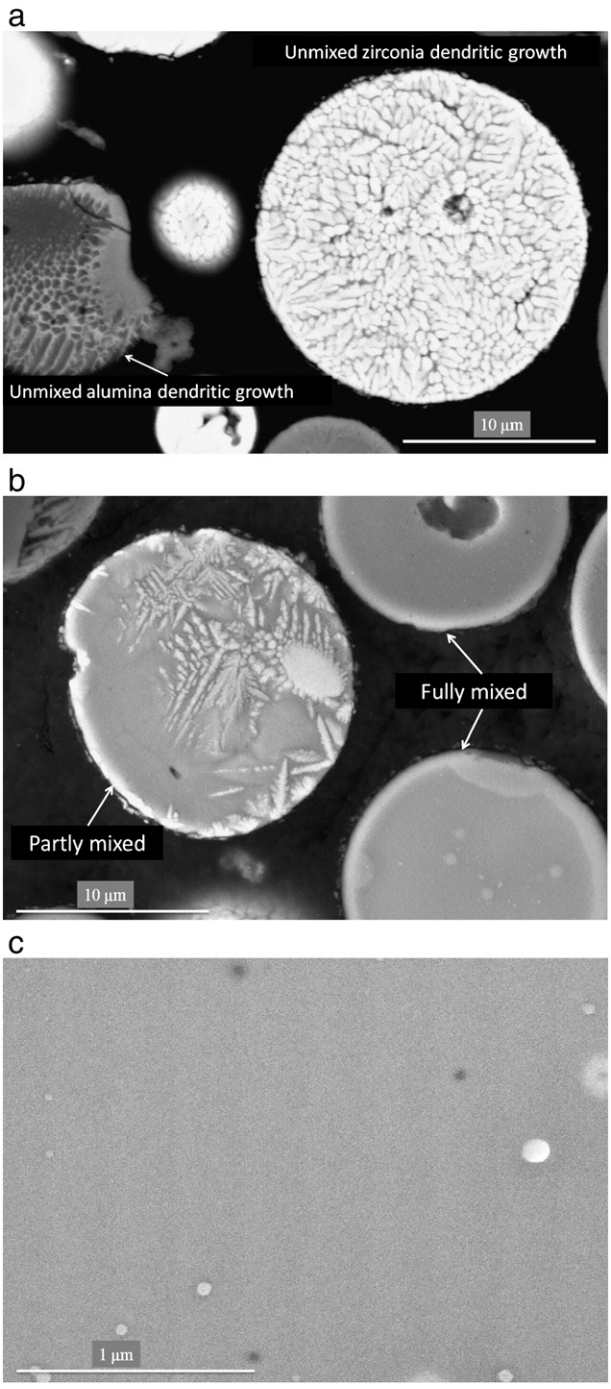

Fig. 5. Cross section of collected in-flight particles of Powder 2 after atmospheric plasma spraying using Mettech Axial III; a) un-mixed dark alumina and white zirconia particles with dendritic structure, b) partly-mixed and fully mixed particle and c) high resolution microscopy of the fully mixed particle showing no sign of crystalline grains throughout the particle.

EDS on some of these particles, however, revealed off-eutectic compositions with an atomic ratio of typically 36/11 or 29/41 aluminum to zirconium (eutectic atomic ratio is 1/1). This indicates that the particles with non-eutectic compositions show also a good potential for amorphous phase formation. This is consistent with Ando et al. [18] stating that solid-state immiscibility of alumina and zirconia makes formation of the amorphous phase probable even at compositions far from eutectic. Therefore, the initial composition may be of less importance and highly amorphous structures can even be obtained at off-eutectic compositions.

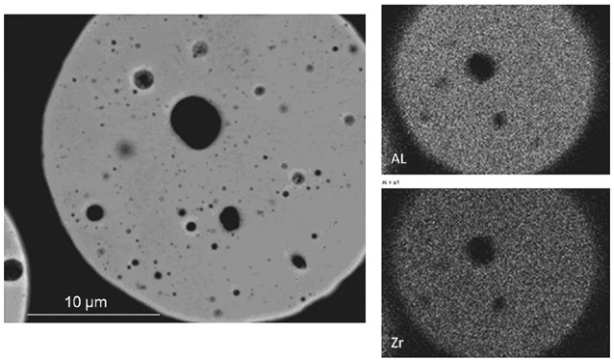

Fig. 6. Fully melted and mixed particle of Powder 2 atmospheric plasma sprayed showing homogenous composition and no sign of crystalline grains with the elemental mapping results for aluminum and zirconium atoms.

It is interesting to note that some in-flight collected particles also showed typical eutectic crystallites and equiaxial cellular grains. An example is shown in Fig. 7 with details of the different regions. Fig. 7(b) shows the particle interior close to the surface, where a fine eutectic structure with about 10 nm alumina and 20 nm YSZ lamella has formed. The particle core in Fig. 7(c) has equiaxed cellular grains of less than 1 μm size with a small pore in the center.

Moreno et al. [19] found eutectic lamella sizes of 50 nm for zirconia and 100 nm for alumina at cooling rates of about 10^3 K/s, while studying rapid solidification of alumina–zirconia melt droplets on copper surfaces. Comparing the lamellae sizes and interpolating linearly, the cooling rate for the present particle can roughly be estimated as 5×10^3 K/s. While many factors, including the particle size, play a role, this comparison suggests a much lower cooling rate for the in-flight solidified particles than for the actual coating splat, which can be more than 10^6 K/s [20].

Close examination of the interface between the two crystal structure in Fig. 7(d) reveals that the thickness of the eutectic lamella does not change with the distance from the interface. This indicates that the reason for the formation of the cellular grains is not the decrease in the cooling rate from the outer to inner parts. This rather suggests that early solidification in the center has originated from pores acting as nucleation sites. It is assumed, in this scenario, that the entire bulk of the molten particle is at temperatures below the melting point. However, the particle core is less undercooled than the regions close to the surface. Contributing to this is the low thermal conductivity of the material that makes it difficult to rapidly homogenize the temperature in the particle. The solidification front originated from the pores has faced the solidification front that started from outside and the two solidification fronts have come to rest at the interface.

The homogeneity of the particle further suggests that the cellular grains in the core are supersaturated solid solutions. The EDS results showed an atomic ratio of 13/ 36 of aluminum to zirconium(or 0.36 atomic ratio compared with the solubility limit of less than 0.01 and eutectic composition of 1/1 atomic ratio).Such supersaturation is against what is predicted by the equilibrium phase diagram, which is applicable mainly for low solidification rate, where the solute atoms exceeding the saturation limit can diffuse out to the remaining liquid phase. The occurrence of a supersaturated solid solution in the coating is further investigated in the following section.

3.2. Coatings study

The coatings from Powder 2 and Powder 1 are compared in Fig. 8(a) and (b), respectively. There is a considerable difference in the coating microstructures. The coating from Powder 1 has higher porosity and higher surface roughness, which can be attributed to the

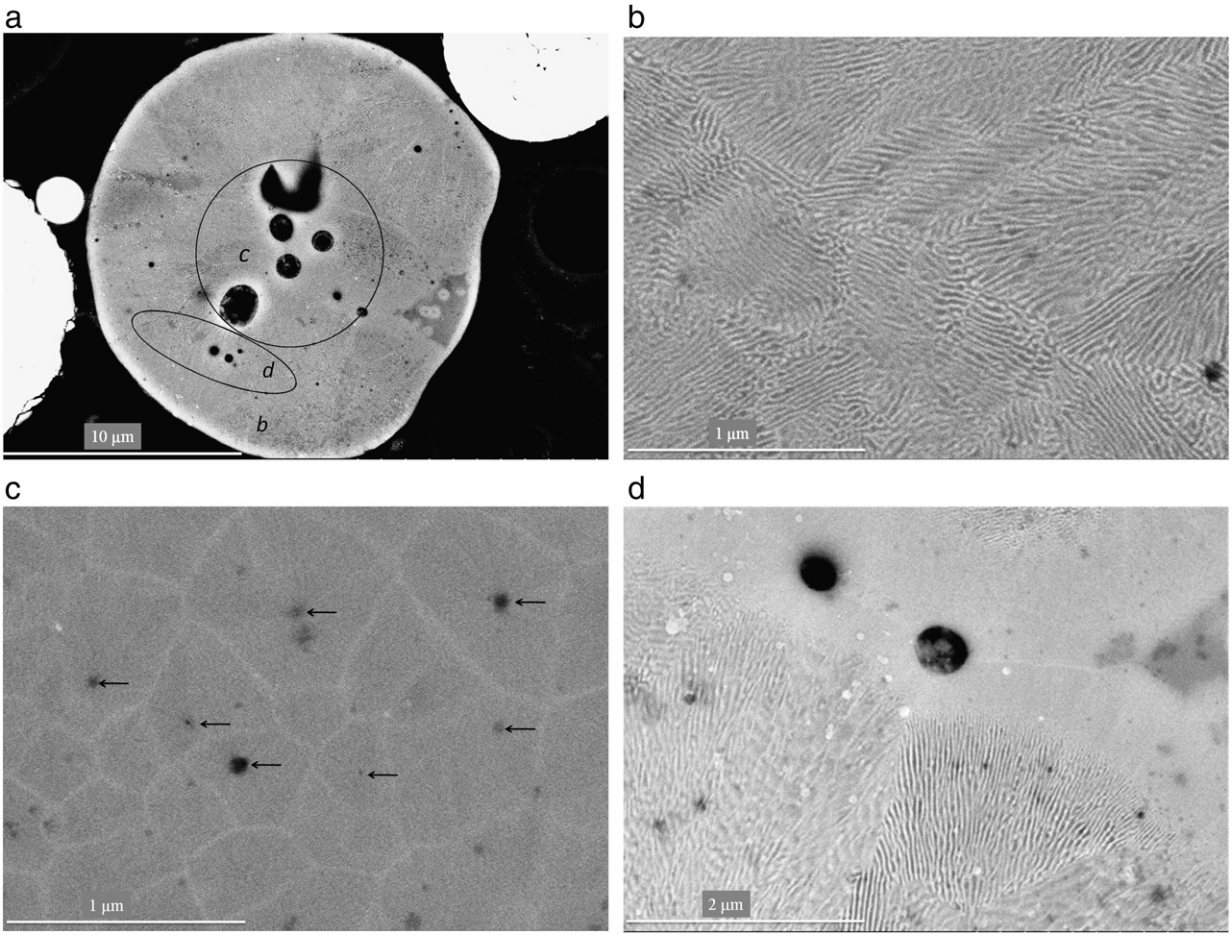

Fig. 7. Structural features in an in-flight particle of sprayed Powder 1, solidified and collected into water a) a typical particle, b) magnified external part designated as *b* in the particle and c) magnified internal part of the particle assigned as *c*, d) interface area of the two phases marked as area *d* in image a.

presence of largely undeformed and shell-like particles with high core porosities.

The inset micrographs in Fig. 8(a) and (b) compare the splats of the two powders at higher magnification. The Powder 2 coating shows distinct dark alumina and bright zirconia splats, in addition to some grey mixed splats. Powder 1 coating, in contrast, shows a uniform structure of grey splats with no clear interfaces. This uniformity is fostered by the intimate contact between the melting particulates.

It can further be noted that in unmelted particles from Powder 1 there is a segregation of zirconia particulates toward the exterior of the particle, leaving a higher concentration of the dark aluminum particulates in the center, as depicted in inset of Fig. 8(b). Those particles are found throughout the coating, as indicated in Fig. 8(b). Such segregation of zirconia and alumina was previously reported for in-flight collected particles, as well as coatings, in suspension plasma spraying [21]. This segregation was only found in the coating and not in the collected particles. The reason for this particle separation is not fully known. The mechanisms in suspension spraying [21] may be different from what is observed here in standard particle spraying.

Complete mixing provides an ideal condition for amorphous phase formation by intimate contact between dissimilar particles. Thus, the structure resulting from well-melted particles shows high uniformity. Chances for in-flight mixing seem to be lower for the Powder 2 coating, which features distinct and differently colored lamella of the splats.

On the other hand, Fig. 9 suggests an additional possibility for mixing and amorphous phase formation. Fig. 9(a) shows the SEM micrograph of the interface area of a solidified alumina splat (dark layer) coated by zirconia (light color splat). It can be seen that there is a region of alumina mixed with zirconia (shown by arrows in this figure) just below the interface. This could have occurred by re-melting of the alumina from the heat input of the oncoming molten zirconia particle (T_m is 2050 °C for alumina and 2700 °C for zirconia).

In contrast, Fig. 9(b) shows the interface when an alumina splat is deposited over the solidified zirconia splat. The distinct separating line between the two splats shows that in this case such mixed region has not formed. Bartuli et al. [22] have reported amorphous phase formation at the interface of a zirconia splat on a solid NiCoCrAlY surface. This was shown to be the result of re-melting and intermixing of aluminum and other bound coat elements into the zirconia splat.

In mixing and amorphous phase formation upon impact, it should be considered that the total area of the interfaces is very limited in comparison with the volume of the splats. In addition, it appears to be mainly the splat with higher melting point, which causes the intermixing upon impact. Thus, the chances for amorphous phase formation by impact should be considerably lower than that due to in-flight mixing.

3.3. Phase analysis

In the DSC measurements, the crystallization peak of the Powder 1 coating showed approximately double the peak area (109 units) than the Powder 2 coating (49 units). This higher amorphous content can be attributed to the intimate contact between the dissimilar nanometric size constituents.

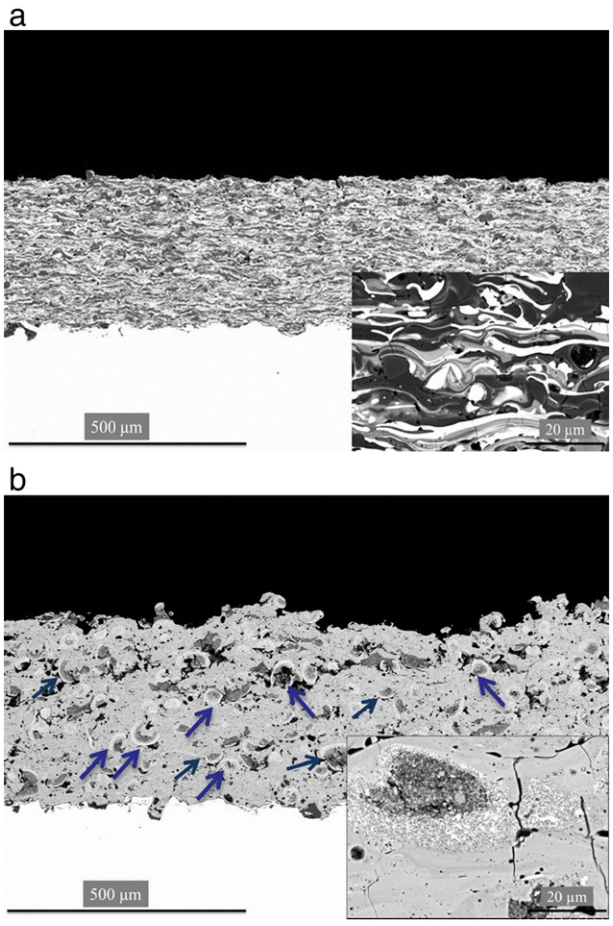

Fig. 8. Coatings microstructures a) using Powder 2, 60/40 alumina/zirconia and b) Powder 1 60/40 alumina/3YSZ powder.

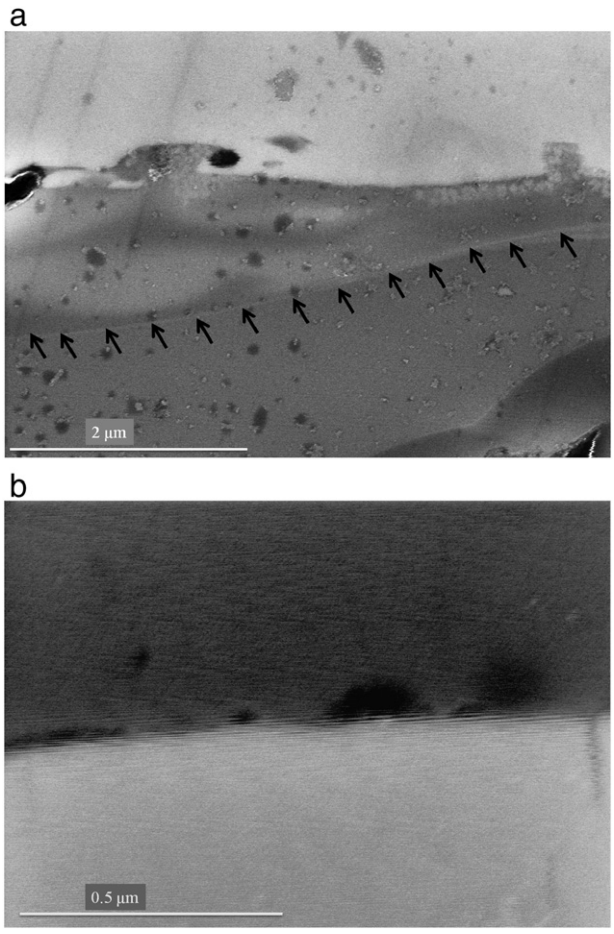

Fig. 9. Intersplat condition a) zirconia splat deposited on solidified alumina splat and b) alumina splat on solidified zirconia in the coatings of Powder 2.

Based on XRD results, the estimated amount of amorphous phase for the Powder 1 coating is less than 44 vol.%. Using image analysis on the micrographs, the unmolten portion of this coating is less than 25 vol.%. The balance of material that is neither amorphous nor unmolten equals to 31 vol.%, likely in the form of a solid solution. Lattice parameter variations, which can give some further insight, will be discussed later in this paper.

Fig. 10 compares the XRD spectra of the coatings with a conventional 7YSZ coating, which was deposited at the same spray conditions. In Fig. 10(a), the zirconia shows a tetragonal structure typical for an YSZAPS coating [23,24]. The Powder 1 coating in Fig. 10 (b) also shows only the tetragonal phase, even though it contains only 3 mol% yttria (partial stabilization). In this coating, the additional stabilizing role of alumina dissolution in this structure has completely prevented any formation of monoclinic zirconia. By contrast, the XRD pattern of the Powder 2 coating in Fig. 10(c) shows a considerable amount of monoclinic phase. This is likely due to a number of factors, such as unmolten feed powder, the absence of an yttria stabilizing agent and the lack of extended dissolution of alumina in zirconia, as was earlier suggested while considering the corresponding microstructures in Fig. 8(a).

Enhanced solubility in the solids, as observed in the in-flight particles, can also be seen in the coatings by shifts in the characteristic XRD peaks of the parent material due to changes in the lattice parameter [25]. Substitution of zirconium or yttrium atoms by smaller aluminum atoms shrinks the unit cell of the YSZ structure. The other possibility is the allocation of aluminum atoms into the interstitial positions of the YSZ structure (either cubic or tetragonal), which would result in an expansion of the unit cell. The former case causes a positive peak shift while the latter results in a negative peak shift toward smaller angles. Thus, the peak shift depends on YSZ crystal structure and the atomic positions that the aluminum atoms take within the unit cell.

Quantitative evaluation of unit cell parameters using Powdercell [17] allows the comparison the aluminum-free 8 wt.% YSZ coating with the Powder 1 coating (60 wt.% alumina in 8 wt.% YSZ), in particular a comparison of the lattice parameters *a* and *c*. It was found

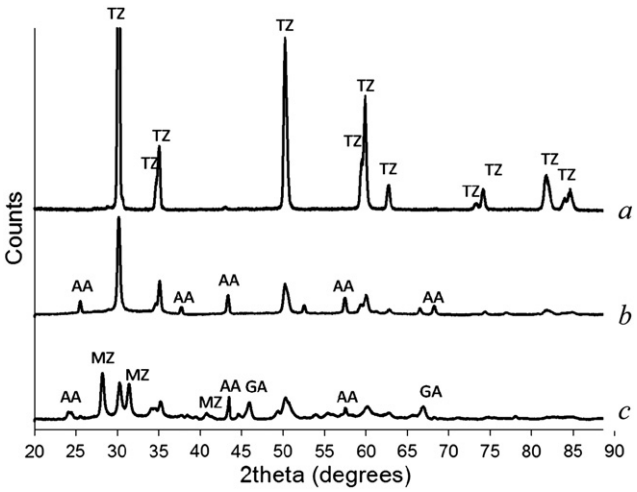

Fig. 10. XRD patterns of the coatings a) YSZ coating with fully tetragonal structure (TZ), b) Powder 2 coating tetragonal zirconia and alpha alumina (AA), c) Powder 1 coating showing (TZ) and monoclinic zirconia (MZ) plus alpha(AA) and gamma alumina (GA).

that parameter *a* decreases from 3.6345 to 3.6306 Å and parameter *c* from 5.1196 to 5.0928 Å. This suggests that significant dissolution of alumina in tetragonal zirconia occurs resulting in reduced lattice parameters. Similar observation was reported by [26] for cubic zirconia, whereby increasing the solubility limit from 4 to 40 mol% alumina, the unit cell of increased from 5.095 to 5.129 Å.

4. Conclusion

In this paper, APS coatings and in-flight collected particles were studied to gain further insight into the formation of crystalline and amorphous phases in plasma sprayed alumina–zirconia composites. It was observed that the sizes of the feed and the collected particles after spraying were similar. This indicates that no considerable fragmentation of the particles in the plasma jet has taken place. In the process, feed particles with intimately mixed constituents gave rise to amorphous structures in the collected particles, even at compositions far from eutectic. For the coatings, two main avenues for amorphous phase formation are proposed: in-flight and upon-impact mixing. It was found that large uniform nano-agglomerated powders are more prone to produce amorphous coatings than micron sized fused and crushed powders.

In addition to amorphisation, the formation of a supersaturated solid solution was noticed. At low solidification rates in the core of collected particles, cellular crystal grains nucleate on residual pores. Without releasing their excessive solute atoms, these grains arrest at the eutectic solidification front, which moves inwards from the particle surface. The existence for such phase was supported by unit cell parameter estimations based on XRD measurements of the coatings. It was found that the dissolution of the aluminum in the zirconia crystal is of interstitial nature, and that surprising high ratios of alumina can be incorporated into the zirconia crystal (as high as eutectic composition). This raises new awareness of this source of crystallinity, which is often not considered in sprayed alumina–zirconia coatings.

Finally, the segregation of zirconia from alumina in unmolten nano-agglomerated particles and its migration toward the exterior regions of the particle was observed. Such segregation was previously experienced in in-flight collected and melted particles of alumina–YSZ.

Acknowledgement

The authors would like to thank NSERC for the partial financial support of this work.

References

[1] P. Fauchais, G. Montavon, M. Vardelle, J. Cedelle, Surf. Coat. Technol. 201 (5) (2006) 1908.
[2] P. Fauchais, M. Vardelle, A. Vardelle, L. Bianchi, A.C. Leger, Plasma Chem. Plasma Process. 16 (1) (1996) 99S.
[3] P. Fauchais, J. Phys. D: Appl. Phys. 37 (2004) R86.
[4] L. Wang, Y. Wang, X.G. Sun, J.Q. He, Z.Y. Pan, Y. Zhou, P.L. Wu, Mater. Design 32 (2011) 36.
[5] N. Toplan, U. Saral, Surf. Eng. 25 (7) (2009) 541.
[6] C.J. Friedrich, R. Gadow, T. Schirmer, Thermal Spray Surface Engineering via Applied Research, Proceedings of the 1st International Thermal Spray Conference, 2000, p. 1219.
[7] P. Ramaswamy, S. Seetharamu, K.B.R. Varma, K.J. Rao, Compos. Sci. Technol. 57 (1) (1997) 81.
[8] G. Shanmugavelayutham, S. Yano, A. Kobayashi, Vacuum 80 (11–12) (2006) 1336.
[9] A.M. Limarga, S. Widjaja, T.H. Yip, Surf. Coat. Technol. 197 (1) (2005) 93.
[10] S. Sharafat, A. Kobayashi, Y. Chen, N.M. Ghoneim, Vac. Surf. Eng., Surf. Instrum. Vac. Technol. 65 (2002) 415.
[11] F. Tarasi, M. Medraj, A. Dolatabadi, J. Oberste-Berghaus, C. Moreau, Proceedings of International Thermal Spray Conference, 2009, p. 409.
[12] H.-J. Kim, Y.J. Kim, J. Mater. Sci. 34 (1) (1999) 29.
[13] A. McDonald, S. Chandra, C. Moreau, J. Mater. Sci. 43 (2008) 4631.
[14] T. Chraska, K. Neufussa, J. Dubskya, P. Ctibora, P. Rohan, Ceram. Int. 34 (5) (2008) 1229.
[15] S. Bouaricha, J.-G. Legoux, P. Marcoux, J. Therm. Spray Technol. 13 (3) (2004) 405.
[16] H.J. Kim, K.M. Lim, B.G. Seong, C.G. Park, J. Mater. Sci. 36 (1) (2001) 49.
[17] G.N. Werner Kraus, Powdercell Software for Windows, 2000 (version 2.4).
[18] Y.S.T. Ando, J. Am. Ceram. Soc. 74 (1991) 410.
[19] M.Y.J.M. Calderon-Moreno, J. Eur. Ceram. Soc. 25 (2005) 1369.
[20] P. Fauchais, V. Rat, C. Delbos, J.F. Coudert, T. Chartier, L. Bianchi, IEEE Trans. Plasma Sci. 33 (2,Pt.3) (2005) 920.
[21] J. Oberste Berghaus, J.-G. Legoux, C. Moreau, F. Tarasi, T. Chraska, J. Therm. Spray Technol. 17 (1) (2008) 91.
[22] C. Bartuli, L. Bertamini, S. Matera, S. Sturlese, Mater. Sci. Eng., A 199 (1995) 229.
[23] A.H. King, T. Chraska, Thin Solid Films 397 (2001) 40.
[24] M.A. Golozar, J. Mostaghimi, T.W. Coyle, R. Soltani, Wear Behavior of Nanostructured and Conventional Y-PSZ Coatings, Proceedings of the International Symposium on Materials Degradation: Innovation, Inspection, Control and Rehabilitation, August 21–24, 2005, Calgary, AB, Canada, p. 273.
[25] B.D. Cullity, Structure of Polycrystalline Aggregates, 2nd ed., Addison-Wesley publishing Company, Inc., USA, California, 1978, p. 285.
[26] O. Yamaguchi, M. Shirai, M. Yoshinaka, Commun. Am. Ceram. Soc. 71 (12) (1988) C510.